Supplementary Materials:

Ru nanoclusters confined on α/β cobalt hydroxide nanosheets as efficient bifunctional oxygen electrocatalysts for Zn-air battery

Yu Zhang, ‡[a] Ting Hu, ‡[b] Changwang Ke, [a] Fengyan Han, [a] Weiping Xiao, *[a,c] and Xiaofei Yang *[a]

[a] *College of Science, Institute of Materials Physics and Chemistry, Nanjing Forestry University, Nanjing 210037, China*

[b] *Key Laboratory of Advanced Energy Materials Chemistry (Ministry of Education), College of Chemistry, Nankai University, Tianjin 300071, China*

[c] *School of Science, Nanjing University of Science and Technology, Nanjing 210094, China*

‡ *These authors contributed equally to this work*

*Corresponding author

E-mail address: wpxiao@njfu.edu.cn, xiaofei.yang@njfu.edu.cn

Figure S1 Digital photograph of the mixed $Co(OH)_2$ after 24 h-standing.

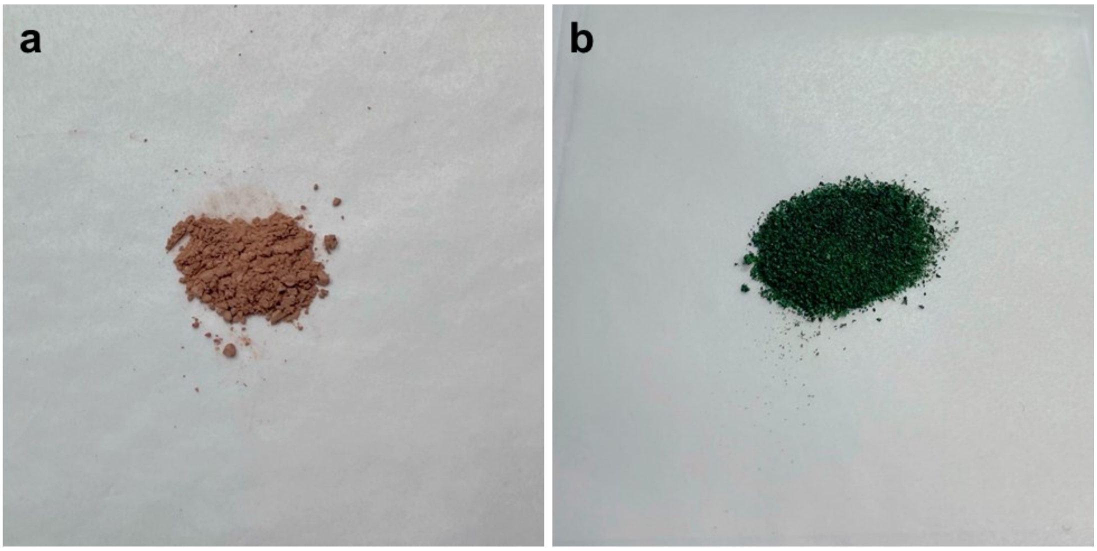

Figure S2 Digital photograph of β-$Co(OH)_2$ (a) and α-$Co(OH)_2$ (b) powders.

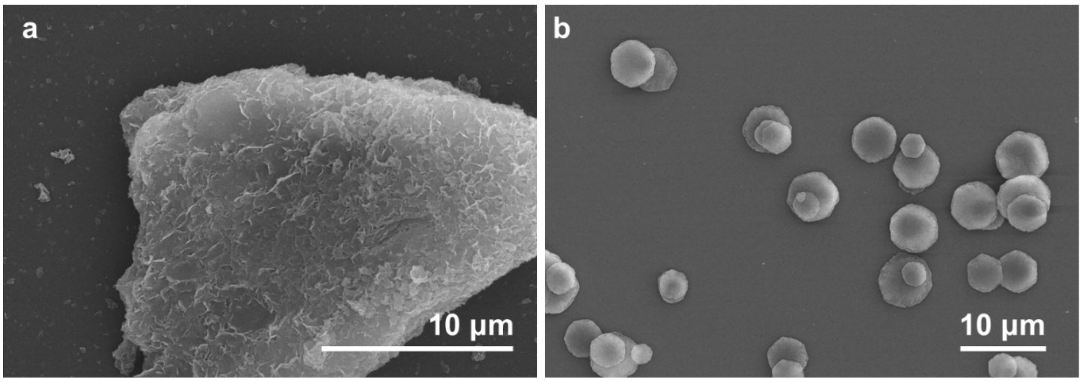

Figure S3 SEM images of (a) α-$Co(OH)_2$, (b) β-$Co(OH)_2$.

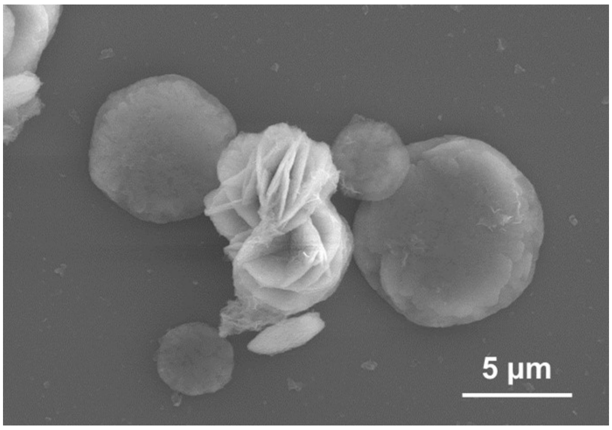

Figure S4 SEM image of mixed phase of $Co(OH)_2$.

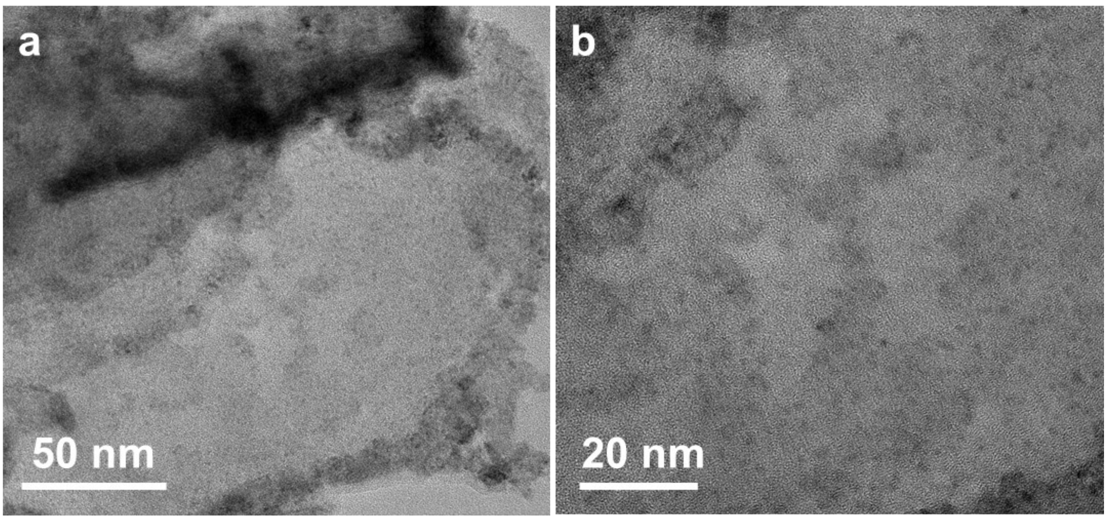

Figure S5 HRTEM images of α-$Co(OH)_2$-Ru.

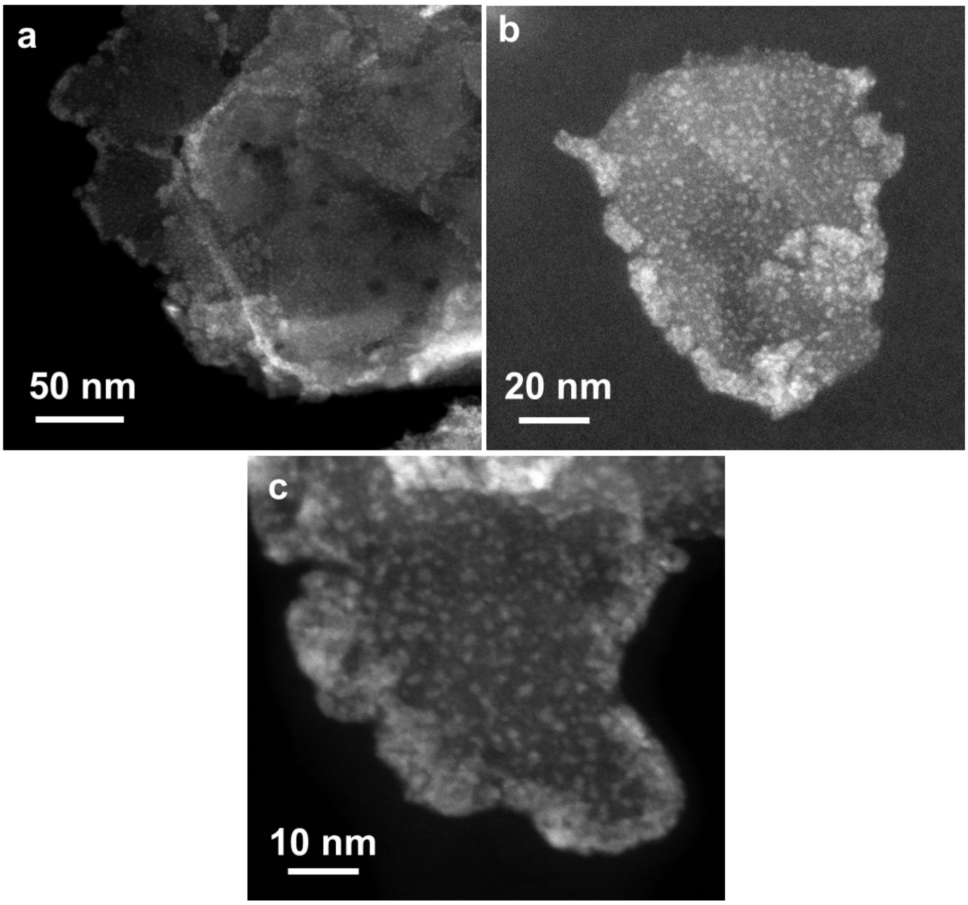

Figure S6 STEM images of α-$Co(OH)_2$-Ru.

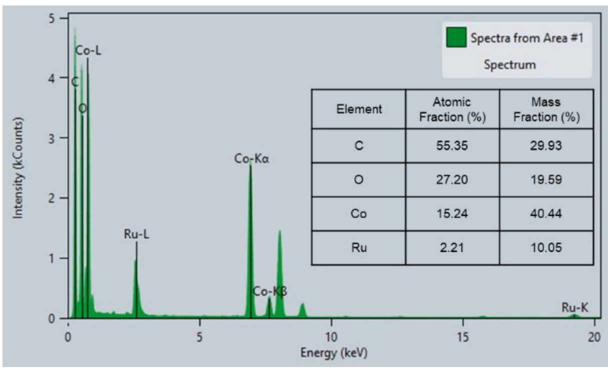

Element	Atomic Fraction (%)	Mass Fraction (%)
C	55.35	29.93
O	27.20	19.59
Co	15.24	40.44
Ru	2.21	10.05

Figure S7 EDX image and corresponding analysis of spectrum of α-$Co(OH)_2$-Ru.

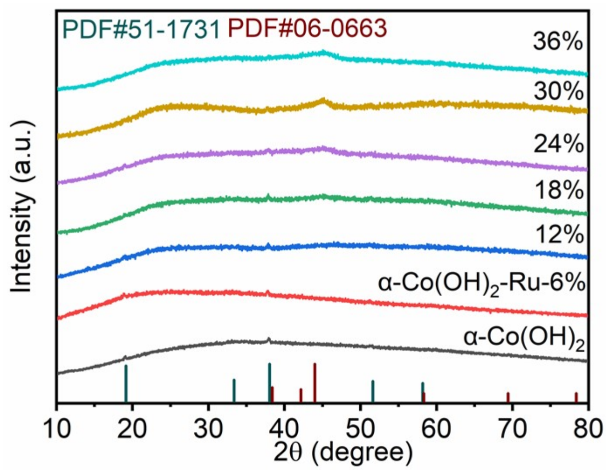

Figure S8 XRD pattern of α-$Co(OH)_2$-Ru with different loadings of Ru.

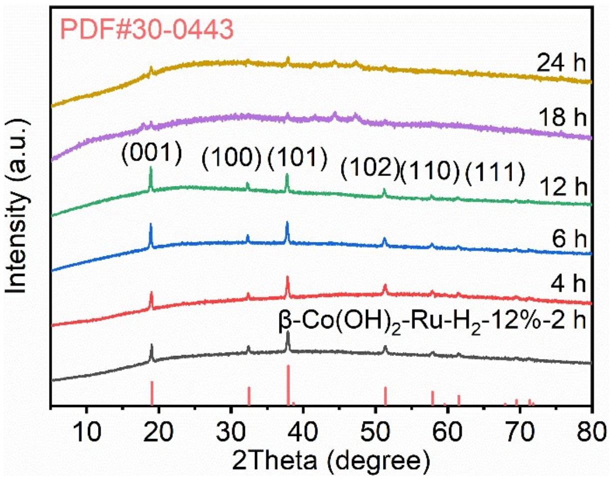

Figure S9 XRD pattern of β-$Co(OH)_2$-Ru with different stirring time.

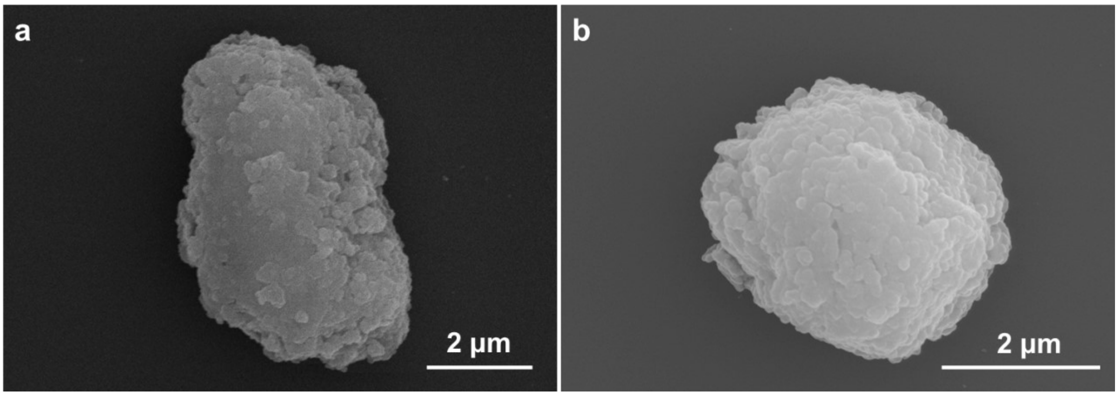

Figure S10 SEM images of α-$Co(OH)_2$-Ru and β-$Co(OH)_2$-Ru after stirring for 18 h.

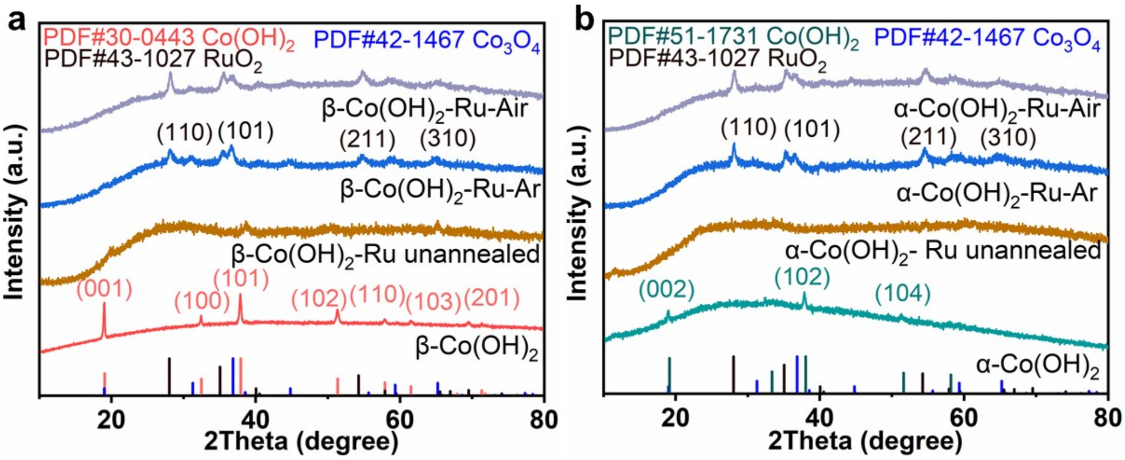

Figure S11 XRD pattern of β-$Co(OH)_2$-Ru α-$Co(OH)_2$-Ru annealed under different atmosphere.

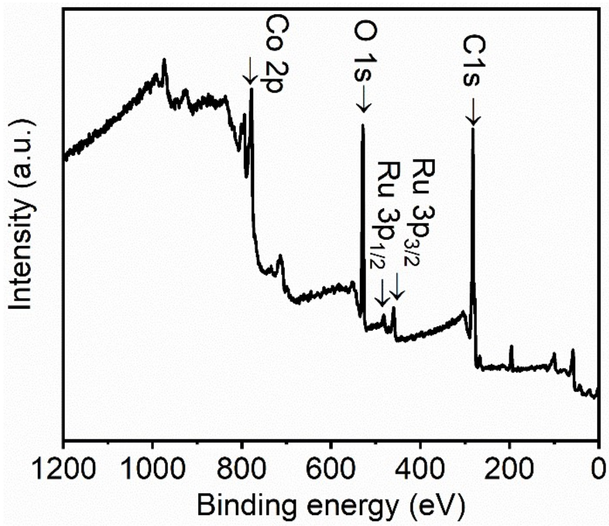

Figure S12 The XPS survey spectra of α-$Co(OH)_2$-Ru.

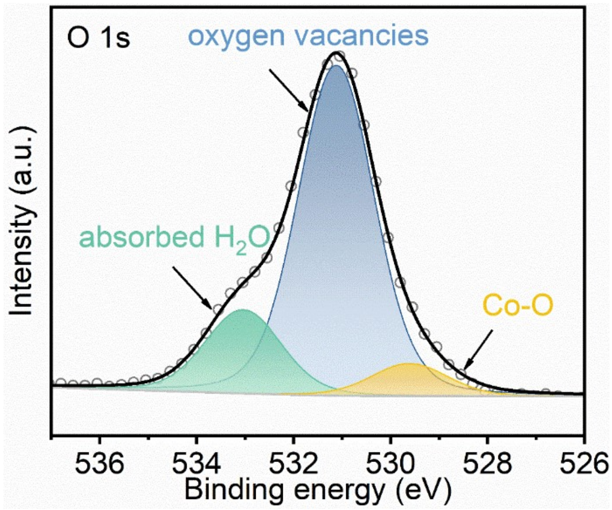

Figure S13 O1s XPS spectrum of α-$Co(OH)_2$-Ru.

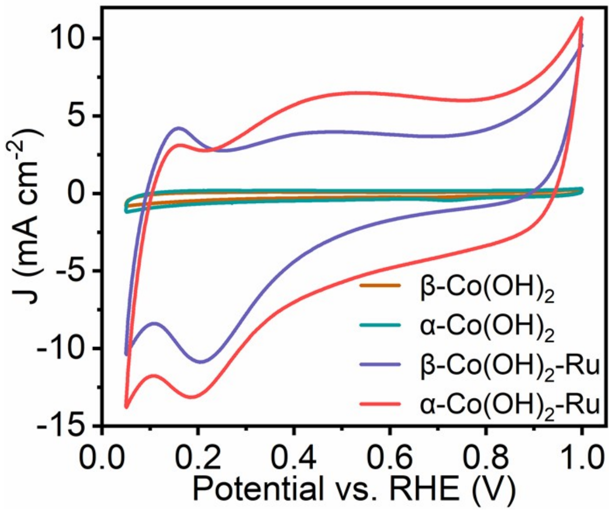

Figure S14 CV curves of different samples at the scan rate of 50 mV s^{-1}.

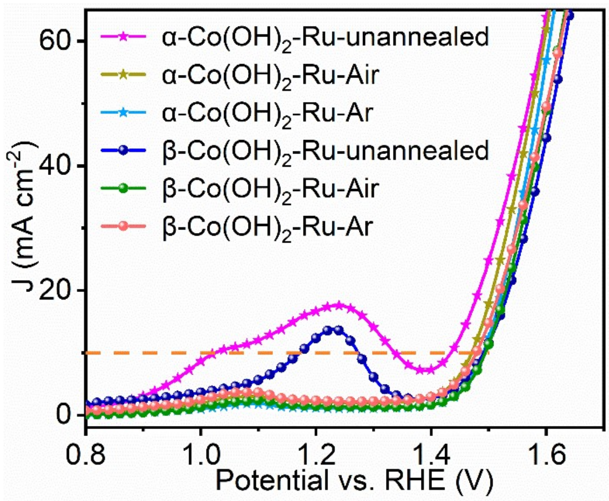

Figure S15 LSV curves of β-$Co(OH)_2$-Ru α-$Co(OH)_2$-Ru annealed under different atmosphere.

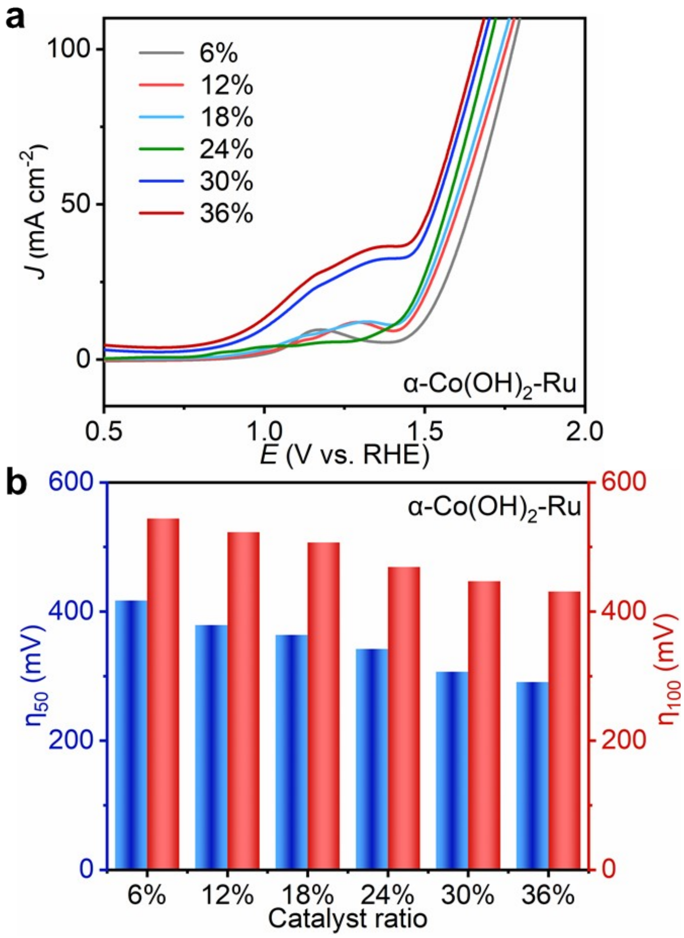

Figure S16 OER performance of α-$Co(OH)_2$-Ru with different Ru loading and its corresponding overpotential @50 mA cm^{-2} (η_{50}), @100 mA cm^{-2} (η_{100}).

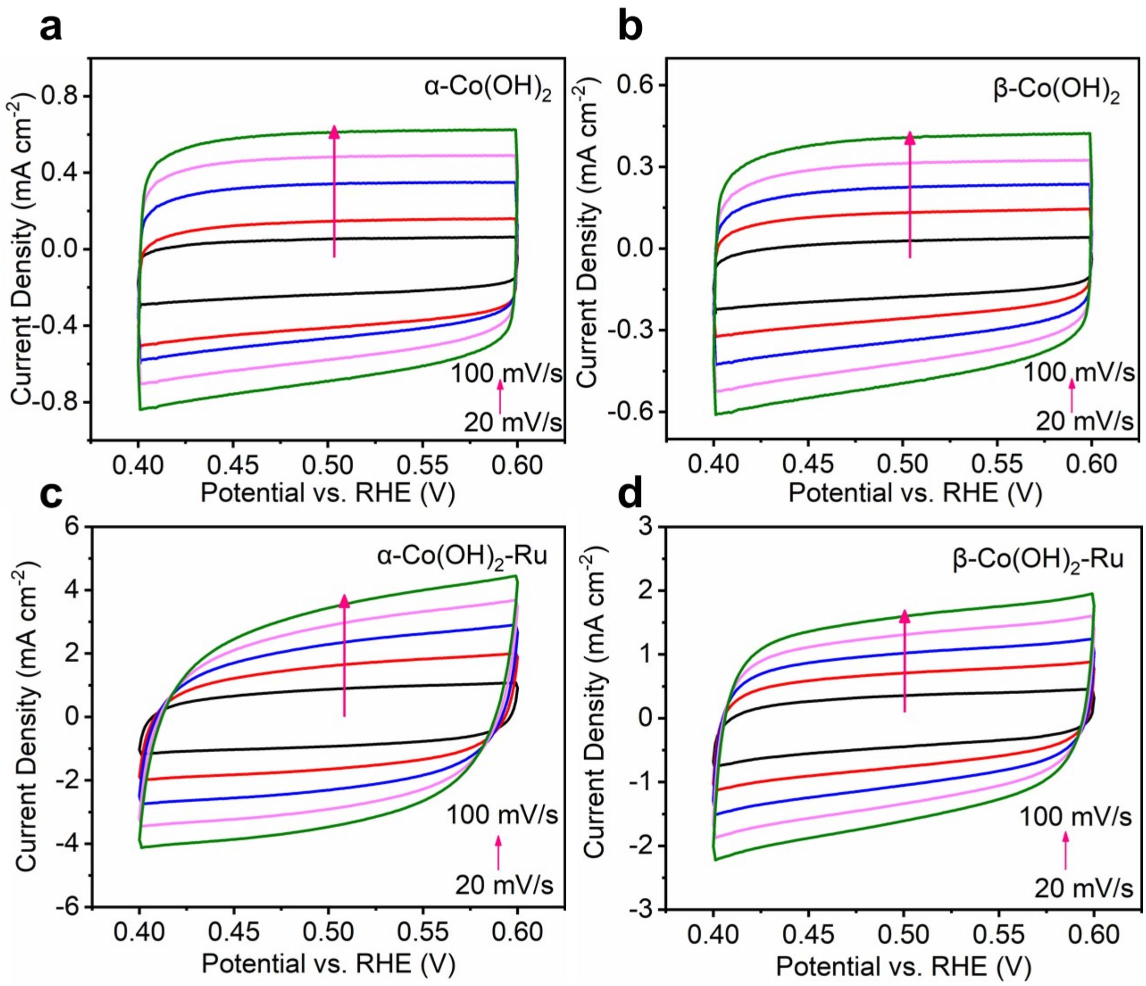

Figure S17 The CV curves of (a) α-$Co(OH)_2$, (b) β-$Co(OH)_2$, (c) α-$Co(OH)_2$-Ru and (d) β-$Co(OH)_2$-Ru in the potential region of 0.4-0.6 V (vs. RHE) in 1 M KOH.

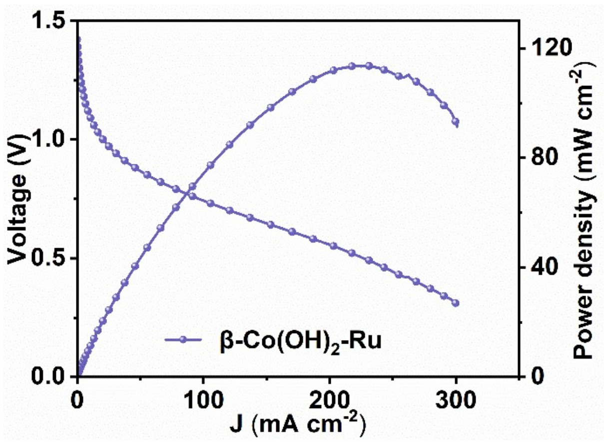

Figure S18 The discharge voltage curve and the corresponding power density plot of β-$Co(OH)_2$-Ru.

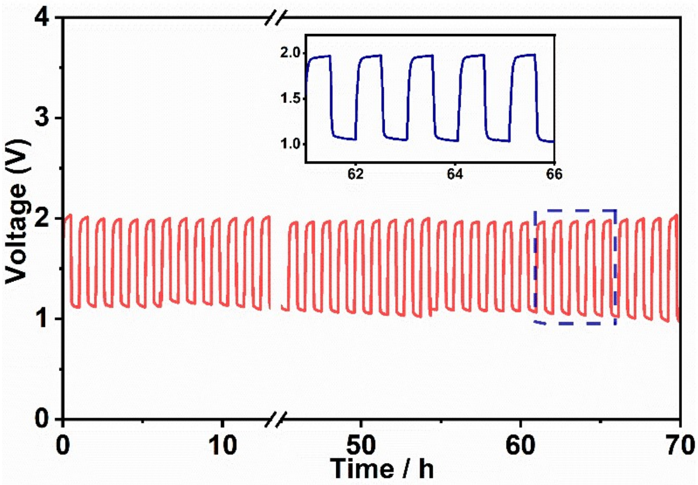

Figure S19 The in-depth discharge/charge plot at 5 mA cm^{-2} followed by 30 min charging and 30 min discharging.

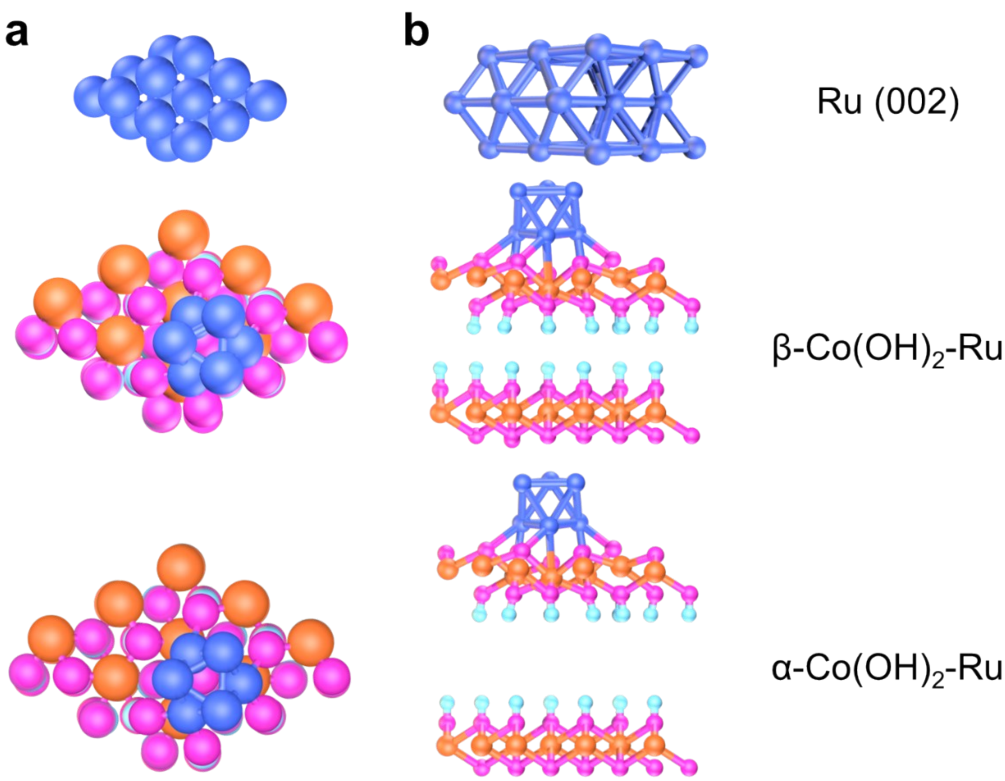

Figure S20 Schematic structure model of Ru (002), β-$Co(OH)_2$-Ru and α-$Co(OH)_2$-Ru from top(a) and side(b) views.

Table S1. Ru content was determined by the ICP-OES analysis for the α-$Co(OH)_2$-Ru and β-$Co(OH)_2$-Ru catalysts.

Samples	**Ru(wt%) (ICP-OES)**
α-$Co(OH)_2$-Ru	0.117
β-$Co(OH)_2$-Ru	0.104

Table S2. The advanced bifunctional ORR/OER catalysts

Samples	**$E_{j=10}$ (V)**	**$E_{1/2}$ (V)**	**ΔE (V)**	**Reference**
α-$Co(OH)_2$-Ru	**1.429**	**0.872**	**0.557**	**This work**
β-$Co(OH)_2$-Ru	**1.465**	**0.851**	**0.614**	**This work**
Mn-RuO_2	1.498	0.862	0.636	1
$Bi_2Ru_2O_7$	1.68	0.83	0.85	2
$La_{1.5}Sr_{0.5}NiMn_{0.5}Ru_{0.5}O_6$	1.66	0.73	0.93	3
Ru-FeRu@C/NC	1.575	0.900	0.675	4
Ru-RuO_2@NPC	1.52	0.86	0.56	5
Ru@Co_3O_4-1.0	1.61	0.77	0.84	6
Ru–Cl–N SAC	1.463	0.9	0.563	7
Ca_2FeRuO_6	1.63	0.78	0.85	8
CoRu-O/A@HNC-2	1.483	0.821	0.662	9
RuO_x-nc@Co_3O_4-250	1.51	0.8	0.71	10
Co-Fe-Ru/PNCS	1.54	0.843	0.697	11
RuCo/NPC	1.58	0.8	0.78	12

References

1 C. Zhou, X. Chen, S. Liu, Y. Han, H. Meng, Q. Jiang, S. Zhao, F. Wei, J. Sun, T. Tan and R. Zhang, Superdurable Bifunctional Oxygen Electrocatalyst for High-Performance Zinc-Air Batteries, *J. Am. Chem. Soc.*, 2022, **144**, 2694–2704.

2 M. Kim, H. Ju and J. Kim, Single crystalline $Bi_2Ru_2O_7$ pyrochlore oxide nanoparticles as efficient bifunctional oxygen electrocatalyst for hybrid Na-air batteries, *Chem. Eng. J.*, 2019, **358**, 11–19.

3 M. Retuerto, F. Calle-Vallejo, L. Pascual, G. Lumbeeck, M. T. Fernandez-Diaz, M. Croft, J. Gopalakrishnan, M. A. Pena, J. Hadermann, M. Greenblatt and S. Rojas, $La_{1.5}Sr_{0.5}NiMn_{0.5}Ru_{0.5}O_6$ Double Perovskite with Enhanced ORR/OER Bifunctional Catalytic Activity, *ACS Appl. Mater. Inter.*, 2019, **11**, 21454–21464.

4 W. Feng, Y. Feng, J. Chen, H. Wang, Y. Hu, T. Luo, C. Yuan, L. Cao, L. Feng and J. Huang, Interfacial electronic engineering of Ru/FeRu nanoparticles as efficient trifunctional electrocatalyst for overall water splitting and Zn-air battery, *Chem. Eng. .J.*, 2022, **437**, 135456–135466.

5 N. Wang, S. Ning, X. Yu, D. Chen, Z. Li, J. Xu, H. Meng, D. Zhao, L. Li, Q. Liu, B. Lu and S. Chen, Graphene composites with Ru-RuO_2 heterostructures: Highly efficient Mott–Schottky-type electrocatalysts for pH-universal water splitting and flexible zinc–air batteries, *Appl. Catal. B Environ.*, 2022, **302**, DOI：10.1016/j.apcatb.2021.120838.

6 C. Huang, Q. Ji, H. Zhang, Y. Wang, S. Wang, X. Liu, Y. Guo and C. Zhang, Ru-incorporated Co_3O_4 nanoparticles from self-sacrificial ZIF-67 template as efficient bifunctional electrocatalysts for rechargeable metal-air battery, *J. Colloid Interface Sci.*, 2022, **606**, 654-665.

7 J. Chen, J. Huang, R. Wang, W. Feng, H. Wang, T. Luo, and Y. Hu, L. Feng, L. Cao, K. Kajiyoshi, C. He, Y. Liu, Z. Li, and Y. Feng Atomic ruthenium coordinated with chlorine and nitrogen as efficient and multifunctional electrocatalyst for overall water splitting and rechargeable zinc-air battery, *Chem. Eng. J.*, 2021, **441**, 136078–136088.

8 N. Kumar, K. Naveen, M. Kumar, T. C. Nagaiah, R. Sakla, A. Ghosh, V. Siruguri, S. Sadhukhan, S. Kanungo and A. K. Paul, Multifunctionality Exploration of Ca_2FeRuO_6: An Efficient Trifunctional Electrocatalyst toward OER/ORR/HER and Photocatalyst for Water Splitting, *ACS Appl. Energy Mater.*, 2021, **4**, 1323–1334.

9 G. Li, K. Zheng, W. Li, Y. He and C. Xu, Ultralow Ru-Induced Bimetal Electrocatalysts with a Ru-Enriched and Mixed-Valence Surface Anchored on a Hollow Carbon Matrix for Oxygen Reduction and Water Splitting, *ACS Appl. Mater. Inter.*, 2020, **12**, 51437–51447.

10 Q. Lu, Y. Guo, P. Mao, K. Liao, X. Zou, J. Dai, P. Tan, R. Ran, W. Zhou, M. Ni and Z. Shao, Rich atomic interfaces between sub-1 nm RuO_x clusters and porous Co_3O_4 nanosheets boost oxygen electrocatalysis bifunctionality for advanced Zn-air batteries, *Energy Storage Mater.*, 2020, **32**, 20–29.

11 Z. Peng, C. Han, C. Huang, Z. Dong and X. Ma, Preventing surface passivation of transition metal nanoparticles in oxygen electrocatalyst to extend the lifespan of Zn-air battery, *J. Mater. Sci. Technol.*, 2022, **128**, 205–212.

12 Y. Pei, W. He, M. Wang, J. Wang, T. Sun, L. Hu, J. Zhu, Y. Tan and J. Wang, RuCo alloy trifunctional electrocatalysts with ratio-dependent activity for Zn-air batteries and self-powered water splitting, *Chem. Commun.*, 2021, **57**, 1498–1501.